Article

Goos–Hänchen Lateral Displacements and Angular Deviations: When These Optical Effects Offset Each Other

Stefano De Leo [1,*] [iD] **, Luca Maggio** [2] **and Moreno d'Ambrosio** [2]

1   Department of Applied Mathematics, State University of Campinas, Campinas 13083859, Brazil
2   Department of Mathematics and Physics, University of Salento, 73100 Lecce, Italy
*   Correspondence: deleo@unicamp.br

Abstract: For optical beams transmitted by a right-angle prism, the Goos–Hänchen shift can never be seen as a pure effect. Indeed, the lateral displacement, caused by the total internal reflection, will always be accompanied by angular deviations generated by the transmission through the incoming and outgoing interfaces. This combined effect can be analyzed by using the Taylor expansion of the Fresnel coefficients. The analytic expression found for the transmitted beam allows us to determine the beam parameters, the incidence angles, and the axial distance for which lateral displacements are compensated by angular deviations. Proposals to optimize experimental implementations are also briefly discussed.

Keywords: laser; Goos–Hänchen shift; angular deviations

1. Introduction

The interaction between optical beams and dielectric blocks has always been the subject of great interest, leading, in the past, to formulate the well-known laws of geometric optics [1–3]. In the last century, new phenomena such as the Goos–Hänchen shift [4–8] and angular deviations [9] showed that the optical path predicted by geometric optics only represents an approximation to the real one. Theoretical studies have been undertaken in order to understand which situations lateral displacements and angular deviations can be amplified and then observed in the laboratory. The omnipresence of these phenomena [10–14] also stimulated their application in technology [15–17].

In 1947, Goos and Hänchen [4] were the first researchers to experimentally observe the lateral displacement of optical beams transmitted, after many internal reflections, by a dielectric block. The experimental result, today known as Goos–Hänchen shift, was, one year later, explained by Artman [5]. Artmann's observation was that multiple plane waves, contributing to the final electromagnetic field, have rapidly varying phases that cancel each other out. Total internal reflection is indeed characterized by a complex Fresnel coefficient. The stationary condition gives the main term of the phase which is responsible for the additional phase generating the lateral shift in the optical path [18]. The divergence in the Artmann formula was later removed [6,7]. Recently, for incidence in the critical region, an analytical formula, based on the modified Bessel functions, was proposed in [8] and, some years later, experimentally confirmed [19].

In 1973, Ra, Bertoni, and Felsen [9] introduced the phenomenon of angular deviation. This phenomenon appears both for transmission (in this case, we have deviations from the refraction angle predicted by the Snell law) and partial reflection (in this case, we find deviations from the reflected angle predicted by the reflection law). This phenomenon is due, essentially, to the symmetry breaking of the Gaussian distribution caused by the Fresnel coefficients modulating the Gaussian distribution in the integral form of the transmitted and reflected beams.

Angular deviations and Goos–Hänchen shifts have been investigated in great detail in different fields, not only in optics [10–12,15,17] but also in seismic data analysis [13,14]. In

the critical region, lateral displacements and angular deviations generate oscillatory phenomena, theoretically predicted in [20] and, recently, experimentally confirmed in [21,22].

In this article, we analyze the combined effect of the angular deviations (caused by the transmission through the incoming and outgoing triangular prism interfaces) and the Goos–Hänchen shift (caused by the total internal reflection). The study is done outside the critical region. This choice is justified because, outside the critical region, we have the possibility to find an analytic expression for the transmitted beam by using the Taylor expansion of the Fresnel coefficients and, consequently, determine the beam parameters, the incidence angles, and the axial distance for which angular deviations compensate Goos–Hänchen lateral displacements. The integral form of the beam transmitted through a dielectric prism, see Figure 1a, is characterized by three Fresnel coefficients: the ones corresponding to the transmission at the left (air/dielectric) and right (dielectric/air) interfaces and the one corresponding to the total internal reflection at the lower (dielectric/air) interface. The upper transmitted beam is, thus, the perfect candidate to study the combined effect of angular deviations and Goos–Hänchen shifts. In the next section, we fix our notation, introduce the Fresnel coefficients, and calculate the phase of the optical beams. The integral form of the (upper) transmitted beam cannot be analytically solved, so we use the Taylor expansion of the Fresnel coefficients and of the optical phase to obtain a closed form for the transmitted beam. By using this analytic approximation, we obtain a *cubic equation* which allows us to determine the peak position of the transmitted beam. In a previous paper [23], based on this cubic equation, we studied the phenomenon of pure angular deviations, which implies an incidence angle below the critical one. In this paper, we analyze incidence greater than the critical one. This allows us to investigate both angular deviations and Goos–Hänchen displacements (only present in the case of total internal reflection). In this incidence region, it is thus possible to study when these optical effects offset each other. Discussions, conclusions, and proposals for experimental implementations appear in the final sections.
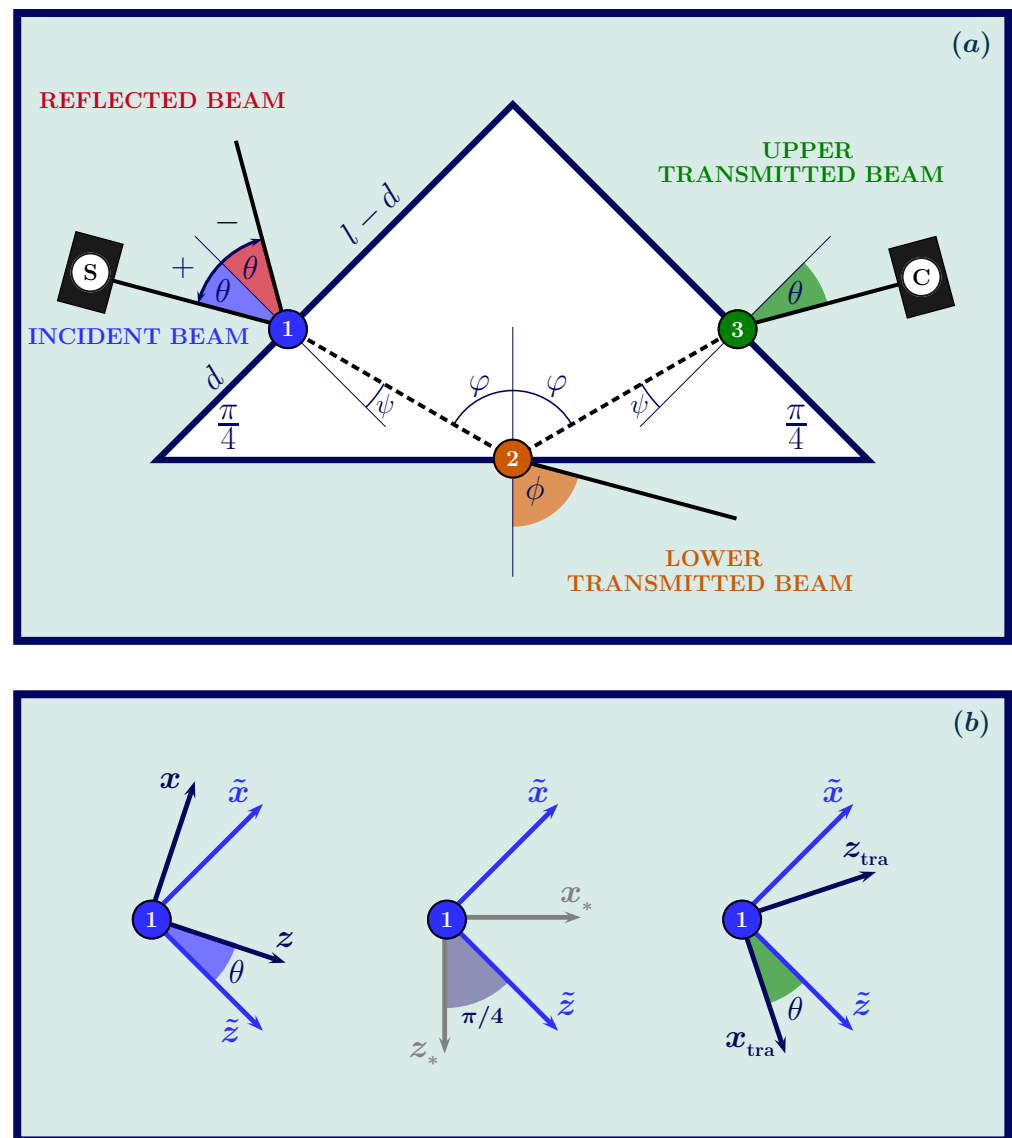
Figure 1. Geometrical layout of the dielectric prism. In (**a**), a laser beam moves, along the *z*-axis, from the source, Ⓢ, to the air/dielectric interface, ❶, forming an incidence angle, θ, with the normal to the first interface, $\tilde{z}$. The beam transmitted through the first interface then moves in the dielectric prism towards the second (dielectric/air) interface, ❷, forming an angle ψ with the normal to the first interface, $\tilde{z}$, and an angle φ with the normal to the second interface, z_*. These angles are related to the incidence one by the Snell law, $\sin\theta = n\sin\psi$ and $n\sin\varphi = \sin\phi$, where $\varphi = \psi + \pi/4$. Once reflected by the second interface, the optical beam moves to the third (dielectric/air) interface, ❸. Due to the geometry of the prism, the upper transmitted beam forms an angle θ with respect to the normal to the third interface, $\tilde{x}$. The upper transmitted beam is thus detected at the camera©. In (**b**), we find the coordinates systems of the incident and upper transmitted beams and of the prism interfaces.

2. The Incident Beam

Let us introduce the integral form of the incident beam

$$E^{[\text{inc}]}(\mathbf{r}) = E_0 \int \mathrm{d}k_x\,\mathrm{d}k_y\; G(k_x, k_y)\; e^{i\,\boldsymbol{k}\cdot\mathbf{r}}\;, \tag{1}$$

where

$$G(k_x, k_y) = \frac{\mathrm{w}_0^2}{4\,\pi}\, \exp\left[-\left(k_x^2 + k_y^2\right)\frac{\mathrm{w}_0^2}{4}\right]$$

is the Gaussian wave number distribution, and

$$\boldsymbol{k} \cdot \mathbf{r} = k_x x + k_y y + k_z z$$

is the optical phase with $|\boldsymbol{k}| = 2\pi/\lambda$. By using the paraxial approximation,

$$k_z \approx |\boldsymbol{k}| - (k_x^2 + k_y^2)/2|\boldsymbol{k}|,$$

the integral in Equation (1) can analytically be solved leading to the following closed expression for the incident Gaussian beam

$$E^{[\text{inc}]}(\mathbf{r}) = \frac{E_0 \, e^{i|\boldsymbol{k}|z}}{1 + i z/z_{\text{R}}} \exp\left[-\frac{x^2 + y^2}{w_0^2(1 + i z/z_{\text{R}})}\right], \tag{2}$$

where $z_{\text{R}} = \pi w_0^2/\lambda$ is the Rayleigh axial range and w_0 the beam waist. The beam intensity is then given by

$$I^{[\text{inc}]}(\mathbf{r}) = I_0 \frac{w_0^2}{w^2(z)} \exp\left[-2\frac{x^2 + y^2}{w^2(z)}\right], \tag{3}$$

where $I_0 = E_0^2$ and $w(z) = w_0 \sqrt{1 + (z/z_{\text{R}})^2}$.

3. The Optical Phase

In the integral form of optical beams, an important role is played by the optical phase responsible for the optical path of the beam. In order to calculate the optical phase of the (upper) transmitted beam, it is useful to introduce the coordinate system corresponding to the incident and transmitted beams and the ones corresponding to the left, right, and lower interfaces, see Figure 1b,

$$\begin{pmatrix} \widetilde{x} \\ \widetilde{z} \end{pmatrix} = M(-\theta) \begin{pmatrix} x \\ z \end{pmatrix} = M\left(\frac{\pi}{4}\right) \begin{pmatrix} x_* \\ z_* \end{pmatrix} = M(\theta) \begin{pmatrix} z_{\text{tra}} \\ x_{\text{tra}} \end{pmatrix},$$

where $M(\theta) = \{\{\cos\theta, -\sin\theta\}, \{\sin\theta, \cos\theta\}\}$ represents the anti-clockwise rotation matrix. The optical phase corresponding to the beam propagating from the source to the first interface is given by

$$Ⓢ \to \text{①} \quad : \quad k_x\,x + k_z\,z = k_{\widetilde{x}}\,\widetilde{x} + k_{\widetilde{z}}\,\widetilde{z},$$

where

$$\begin{pmatrix} k_{\widetilde{x}} \\ k_{\widetilde{z}} \end{pmatrix} = M(-\theta) \begin{pmatrix} k_x \\ k_z \end{pmatrix}.$$

After transmission through the left (air/dielectric) interface, the beam moves, into the dielectric, towards the lower (dielectric/air) interface with the following optical phase

$$\text{①} \to \text{②} \quad : \quad q_{\widetilde{x}}\,\widetilde{x} + q_{\widetilde{z}}\,\widetilde{z} = q_{x_*}\,x_* + q_{z_*}\,z_*,$$

where

$$\begin{pmatrix} q_{\widetilde{x}} \\ q_{\widetilde{z}} \end{pmatrix} = M\left(\frac{\pi}{4}\right) \begin{pmatrix} q_{x_*} \\ q_{z_*} \end{pmatrix},$$

with

$$q_{\widetilde{x}} = k_{\widetilde{x}} \quad \text{and} \quad q_{\widetilde{z}} = \sqrt{n^2\,|\boldsymbol{k}|^2 - q_{\widetilde{x}}^2 - k_y^2}.$$

The beam is then reflected back and moves between the lower and right interface with an optical phase given by

$$\text{②} \to \text{③} \quad : \quad q_{x_*}\,x_* - q_{z_*}\,z_* = q_{\widetilde{x}}\,\widetilde{z} + q_{\widetilde{z}}\,\widetilde{x}.$$

Finally, in the integral form of the (upper) transmitted beam appears, as expected, the following optical phase

$$\text{③} \rightarrow \text{©} : \quad k_{\tilde{x}}\,\tilde{z} + k_{\tilde{z}}\,\tilde{x} = k_x\,x_{\text{tra}} + k_z\,z_{\text{tra}} .$$

4. The Upper Transmitted Beam

Once obtained the optical phase of the upper transmitted beam, we can write its integral form:

$$E_{\text{pol}}^{[\text{tra}]}(\mathbf{r}_{\text{tra}}) = E_0 \int dk_x\,dk_y\; G_{\text{pol}}^{[\text{tra}]}(k_x,k_y)\; e^{i\,\mathbf{k}\cdot\mathbf{r}_{\text{tra}}} , \tag{4}$$

where $\mathbf{r}_{\text{tra}} = (x_{\text{tra}}, y, z_{\text{tra}})$ and

$$G_{\text{pol}}^{[\text{tra}]}(k_x,k_y) = T_{\text{pol}}(k_x,k_y)\,G(k_x,k_y) ,$$

with

$$T_{\text{pol}}(k_x,k_y) = \frac{4\,k_{\tilde{z}}q_{\tilde{z}}}{(a_{\text{pol}}k_{\tilde{z}} + q_{\tilde{z}}/a_{\text{pol}})^2}\,\frac{q_{z_*}/a_{\text{pol}} - a_{\text{pol}}k_{\tilde{z}}}{q_{z_*}/a_{\text{pol}} + a_{\text{pol}}k_{z_*}} \times$$
$$\exp\{i\,[\,q_{z_*}d\,\sqrt{2} + (q_{\tilde{z}} - k_{\tilde{z}})(l - d)\,]\} ,$$

($a_{\text{tm}} = n$ and $a_{\text{te}} = 1$). The additional phase appearing in the Fresnel coefficients is due to the fact that the discontinuities at the air/dielectric and dielectric/air interfaces are located at different points. This phase is responsible for the optical path predicted by geometric optics.

In order to integrate Equation (4), we use the first-order Taylor expansion of the transmission coefficient, i.e.,

$$T_{\text{pol}}(k_x,k_x) = T_{\text{pol}}(0,0)\left[1 + \beta_{\text{pol}}\frac{k_x}{|\mathbf{k}|}\right] \times$$
$$\exp[-i\,k_x\,x_{\text{Snell}}] , \tag{5}$$

where

$$T_{\text{pol}}(0,0) = \frac{4\,n\cos\theta\,\cos\psi}{(a_{\text{pol}}\cos\theta + n\cos\psi/a_{\text{pol}})^2} \times$$
$$\frac{n\cos\varphi/a_{\text{pol}} - a_{\text{pol}}\cos\phi}{n\cos\varphi/a_{\text{pol}} + a_{\text{pol}}\cos\phi} \times$$
$$\exp\{i\,[\,n\cos\varphi\,d\,\sqrt{2} + (n\cos\psi - \cos\theta)(l - d)\,|\mathbf{k}|\,]\}$$

and

$$x_{\text{Snell}} = (\tan\psi\cos\theta - \sin\theta)\,l + (\cos\theta + \sin\theta)\,d .$$

The β_{pol} factor in (5) can be expressed in terms of three addends, respectively corresponding to the transmission through the left (air/dielectric) interface, ①, to the reflection by the lower (dielectric/air) interface, ②, and, finally, to the transmission through the right (dielectric/air) interface, ③,

$$\beta_{\text{pol}} = \beta_{\text{pol}}^{[1]} + \beta_{\text{pol}}^{[2]} + \beta_{\text{pol}}^{[3]} ,$$

with

$$\begin{aligned}
\beta_{\text{te}}^{[1]} &= \tan\psi - \tan\theta \, , \\
\beta_{\text{te}}^{[2]} &= 2\tan\phi\,\varphi' \, , \\
\beta_{\text{te}}^{[3]} &= (\tan\theta - \tan\psi)\,\psi' \, , \\
\beta_{\text{tm}}^{[1]} &= (\tan\psi - \tan\theta/n^2)\,/\,(\sin^2\psi - \cos^2\theta) \, , \\
\beta_{\text{tm}}^{[2]} &= 2\tan\phi\,\varphi'\,/\,(\sin^2\phi - \cos^2\varphi) \, , \\
\beta_{\text{tm}}^{[3]} &= (\tan\theta - n^2\tan\psi)\,\psi'\,/\,(\sin^2\theta - \cos^2\psi) \, ,
\end{aligned}$$

where the different angles which appear in the previous formulas are related to the incidence angle θ by the Snell law, i.e., $\sin\theta = n\sin\psi$ and $n\sin\varphi = \sin\phi$, the angle φ to ψ by the geometry of the prism, i.e., $\varphi = \psi + \pi/4$. Finally, we have $\varphi' = \psi' = \cos\theta/n\cos\psi$.

By using the Taylor expansion (5), we can analytically solve the integral of Equation (4). The k_x term in the exponential will be responsible for the shift in the x_{tra} coordinate, i.e.,

$$\widetilde{x}_{\text{tra}} = x_{\text{tra}} - x_{\text{Snell}} \, ,$$

centering the Gaussian beam in the optical path predicted by the Snell and reflection laws. The constant term in (5), i.e., $T_{\text{pol}}(0,0)$, leads to the same integration done for the incident, consequently, we obtain the following contribution

$$T_{\text{pol}}(0,0)\ E^{[\text{inc}]}(\widetilde{\mathbf{r}}_{\text{tra}}) \, .$$

The linear term, i.e., $T_{\text{pol}}(0,0)\,\beta_{\text{pol}}\,k_x\,/\,|\mathbf{k}|$, is responsible for the breaking of the Gaussian symmetry for incidence below the critical one and for the Goos–Hänchen shift in the case of total internal reflection. Observing that k_x in the integrand of (4) can be replaced by $-i\,\partial/\partial\widetilde{x}_{\text{tra}}$, we obtain the following contribution

$$-i\,T_{\text{pol}}(0,0)\,\frac{\beta_{\text{pol}}}{|\mathbf{k}|}\,\frac{\partial\,E^{[\text{inc}]}(\widetilde{\mathbf{r}}_{\text{tra}})}{\partial\widetilde{x}_{\text{tra}}} \, .$$

The analytical expression for the upper transmitted beam is then given by

$$\begin{aligned}
E_{\text{pol}}^{[\text{tra}]}(\widetilde{\mathbf{r}}_{\text{tra}}) &= \left[1 + 2\,i\,\frac{\beta_{\text{pol}}\widetilde{x}_{\text{tra}}}{|\mathbf{k}|\,\text{w}_0^2\,(1 + i\,z_{\text{tra}}/z_{\text{R}})}\right] \times \\
& \quad T_{\text{pol}}(0,0)\ E^{[\text{inc}]}(\widetilde{\mathbf{r}}_{\text{tra}}) \, .
\end{aligned}$$

Finally, after algebraic manipulations, we find

$$\begin{aligned}
E_{\text{pol}}^{[\text{tra}]}(\widetilde{\mathbf{r}}_{\text{tra}}) &= \left(1 + i\,\frac{\beta_{\text{pol}}\widetilde{x}_{\text{tra}} + z_{\text{tra}}}{z_{\text{R}}}\right) \times \\
& \quad \frac{T_{\text{pol}}(0,0)}{1 + i\,z_{\text{tra}}/z_{\text{R}}}\,E^{[\text{inc}]}(\widetilde{\mathbf{r}}_{\text{tra}}) \, .
\end{aligned} \tag{6}$$

In order to check the validity of our analytical approximation, let us briefly analyze what happens near the critical incidence region. The critical angle is found when $n\sin\varphi_c = 1$, this implies a critical incidence at

$$\theta_c = \arcsin\left[\left(1 - \sqrt{n^2 - 1}\right)/\sqrt{2}\right] \, . \tag{7}$$

In Figure 2, we plot the (upper) transmitted beam shift of the maxima with respect to the path predicted by geometric optics. This is done by numerically integrating Equation (4). The plots of the maxima, as a function of $\delta = (\theta - \theta_c)|\boldsymbol{k}|w_0$, refer to a Gaussian laser with $w_0 = 100\,\mu m$, $\lambda = 532\,nm$, and $n = 1.5195$ (BK7 prism). We can distinguish three regions.
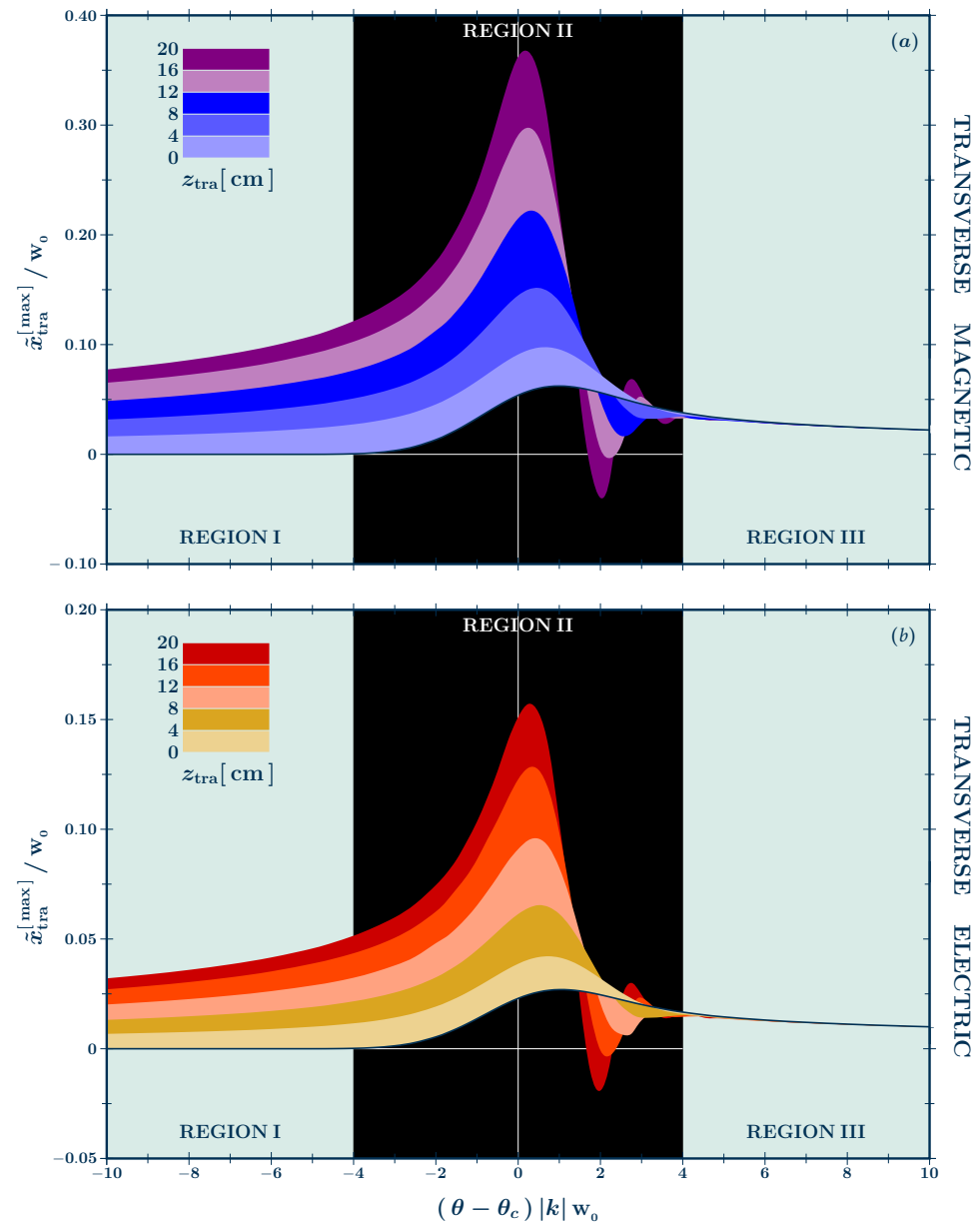
Figure 2. Critical incidence region. Numerical lateral displacements of the maximum of the upper transmitted beam plotted as a function of the incidence angle, $\delta = (\theta - \theta_c)|\boldsymbol{k}|w_0$ for different axial positions both for magnetic (**a**) and electric (**b**) waves. The angular deviations and GH shifts refer to an optical Gaussian beam with $w_0 = 100\,\mu m$, $\lambda = 532\,nm$, and the dielectric block to a BK7 prism, $n = 1.5195$. The black zone represents the critical incidence region in which our analytical approximation fails due to the presence of an infinity in the Taylor expansion. In the incidence region I, $\delta < 4$, and III, $\delta > 4$, our analytical approximations show an excellent agreement with the numerical calculations. In region I, it is clear the axial dependence of the displacement is caused by angular deviations, and in region III the lateral displacement is due to the GH shift. In region III, we do not see any angular deviations because the dominant contribution comes from the Fresnel coefficients of the internal reflection.

Region I, before the critical region, shows an axial dependence of the shift and this is caused by the modulation of the Gaussian wave number function generated by the real Fresnel coefficients related to the transmission through the first and third interface and the partial internal reflection. These phenomena represent angular deviations to the Snell and reflection law of geometric optics. For a detailed discussion of pure angular deviations and their amplifications near the Brewster incidence, we refer the reader to the article cited in [23].

Region II determines the critical region, in such a region the infinity in $\beta_{pol}^{[2]}$ coefficients required a more complicated technique of integration to obtain the analytical expression for the upper transmitted beam [8], and new oscillatory phenomena appear [20,22].

In region III, for incidence greater than the critical one but near enough to amplify the GH shift with respect to angular deviations, this axial depends breaks down. Region III will be the region of interest for our discussion because in this region, far enough from the critical region, angular deviations and GH shifts can offset each other. The analysis in this region complements the one presented in Ref. [23]. In region III, we have

$$\tan\phi = n\,\sin\varphi\,/\,i\,\sqrt{n^2\sin^2\varphi - 1}\ ,$$

and, consequently, the intensity of the upper transmitted beam can be written in the following form

$$I_{pol}^{[tra]}\left(\widetilde{\mathbf{r}}_{tra}\right) = \frac{\mathrm{w}_0^2}{\mathrm{w}^2\left(z_{tra}\right)}\,T_{pol}^2\left(0,0\right)I^{[inc]}\left(\widetilde{\mathbf{r}}_{tra}\right)\times$$

$$\left[\left(1 + \frac{\gamma_{pol}^{[2]}\,\widetilde{x}_{tra}}{z_R}\right)^2 + \left(\frac{z_{tra} + \beta_{pol}^{[1+3]}\,\widetilde{x}_{tra}}{z_R}\right)^2\right]\,, \tag{8}$$

where

$$\gamma_{te}^{[2]} = 2\,\frac{n\,\sin\varphi}{\sqrt{n^2\sin^2\varphi - 1}}\,\cos\theta\,/\,n\,\cos\psi\ ,$$

$$\gamma_{tm}^{[2]} = 2\,\frac{n\,\sin\varphi}{\sqrt{n^2\sin^2\varphi - 1}}\,\frac{\cos\theta\,/\,n\,\cos\psi}{n^2\sin^2\varphi - \cos^2\varphi}\ .$$

and

$$\beta_{pol}^{[1+3]} = \beta_{pol}^{[1]} + \beta_{pol}^{[3]}\ .$$

5. GH Shifts and Angular Deviations

The analytical expression found for the intensity of the upper transmitted beam, see Equation (8), allows us to calculate its maximum and consequently to obtain the lateral displacement with respect to the path predicted by geometric optics due to the GH shifts and angular deviations. The intensity $\widetilde{x}_{tra}$ derivative leads to the following cubic equation

$$\left(\frac{\widetilde{x}_{tra}}{\mathrm{w}_0}\right)^3 + a_{pol}\left(\frac{\widetilde{x}_{tra}}{\mathrm{w}_0}\right)^2 + b_{pol}\,\frac{\widetilde{x}_{tra}}{\mathrm{w}_0} = c_{pol}\ , \tag{9}$$

where

$$a_{pol} = 2 \frac{\gamma_{pol}^{[2]} z_R + \beta_{pol}^{[1+3]} z_{tra}}{\left(\gamma_{pol}^{[2]\,2} + \beta_{pol}^{[1+3]\,2}\right) w_0} \,,$$

$$b_{pol} = \frac{w^2(z)}{w_0^2} \left[\frac{z_R^2}{\left(\gamma_{pol}^{[2]\,2} + \beta_{pol}^{[1+3]\,2}\right) w_0^2} - \frac{1}{2} \right] \,,$$

$$c_{pol} = \frac{w^2(z)}{w_0^2} \frac{\gamma_{pol}^{[2]} z_R + \beta_{pol}^{[1+3]} z_{tra}}{2 \left(\gamma_{pol}^{[2]\,2} + \beta_{pol}^{[1+3]\,2}\right) w_0} \,.$$

This equation allows us to calculate and compare the lateral displacements in region III. When the GH shifts dominate, no axial dependence can be seen. When the angular deviations become comparable with GH shifts an axial dependence is seen in the lateral displacements.

Equation (9) can be reduced to a linear equation by observing that $\widetilde{x}_{tra} \ll w_0$ and that $b_{pol} \gg a_{pol}$ for axial distance $z_{tra} \ll z_R^2 / w_0$. The lateral displacement of the maximum is then given by

$$
\begin{aligned}
\widetilde{x}_{tra}^{[max]} &= c_{pol}\, w_0\, /\, b_{pol} \\
&\approx \frac{\gamma_{pol}^{[2]} + \beta_{pol}^{[1+3]}\, z_{tra}\, /\, z_R}{|k|} \,,
\end{aligned}
\tag{10}
$$

where the axial independent term, proportional to λ, represents the pure GH shift [4,5] and the axial dependent the angular deviations due to the Fresnel transmission modulation of the Gaussian wave number distribution.

Near the critical region,

$$\theta = \theta_c + \delta\, /\, |k| w_0 \qquad [\,\delta \geqslant 4\,],$$

we have

$$n^2 \sin^2 \varphi - 1 \approx 2\, n \cos \varphi_c\, \varphi_c'\, \delta\, /\, |k| w_0 \,.$$

In the example analyzed in this paper, i.e., $\lambda = 532\,\text{nm}$ and $w_0 = 100\,\mu\text{m}$, $\delta \geqslant 4$ implies and incidence angle greater than $\theta_c + 0.2^{\circ}$.

Observing that

$$\beta_{pol}^{[1+3]} \ll \gamma_{pol}^{[2]} \propto \sqrt{|k|\, w_0} \,,$$

and using the approximated expression for the γ factors, we obtain

$$\widetilde{x}_{tra}^{[max]} = \frac{\sigma_{pol}}{n} \sqrt{\frac{2 \cos \theta_c}{\delta \cos \varphi_c \cos \psi_c} \frac{w_0}{|k|}} \,,
\tag{11}$$

with $\{\, \sigma_{te}\,,\, \sigma_{tm}\, \} = \{\, 1\,,\, n^2\, \}$.

Clearly, the axial dependence has been removed and this agrees with the numerical calculation shown in Figure 2, see region III at the right of the black zone. In this region, Equation (11) also contains the well-known $\sqrt{|k|\, w_0}$ amplification for the GH shift, for details see Refs. [8,24]. The σ factor is, finally, responsible for a further amplification of n^2 for the transverse magnetic wave, see the scale in Figure 2a,b.

For transverse magnetic waves, the pure Goos–Hänchen shift is found for incidence at the Brewster angle, i.e.,

$$\beta_{\text{tm}}^{[1+3]} = 0 \;\; \Rightarrow \;\; \theta = \theta_{\text{B}} = \arctan n \; ,$$

see Figure 3a. For a given axial distance, from Equation (10), we can obtain the incidence angle for which the GH shift is compensated by the angular deviation. For example, for a camera positioned at an axial distance of

$$4, 8, 12, 16, 20 \;\; \text{cm} \; ,$$

for the optical beam considered in this paper, we find incidence angles of

$$69.86°, 66.65°, 64.89°, 63.72°, 62.87°$$

for transverse magnetic waves, see Figure 3a, and of

$$68.36°, 62.37°, 58.37°, 55.32°, 52.82°$$

for transverse electric waves, see Figure 3b. Equation (10) can be also used to find, for a given incidence angle, the axial distance for which GH lateral displacements and angular deviations offset each other,

$$z_{\text{tra}} \;\; = \;\; -\frac{\gamma_{\text{pol}}^{[2]}}{\beta_{\text{pol}}^{[1+3]}} \; z_{\text{R}} \; . \tag{12}$$

For example, for incidence angles of

$$45°, 50°, 55°, 60°, 65°, 70° \; ,$$

the compensation happens for transverse electric waves at the axial distances

$$38.10, 25.45, 16.47, 10.22, 5.99, 3.23 \;\; \text{cm} \; ,$$
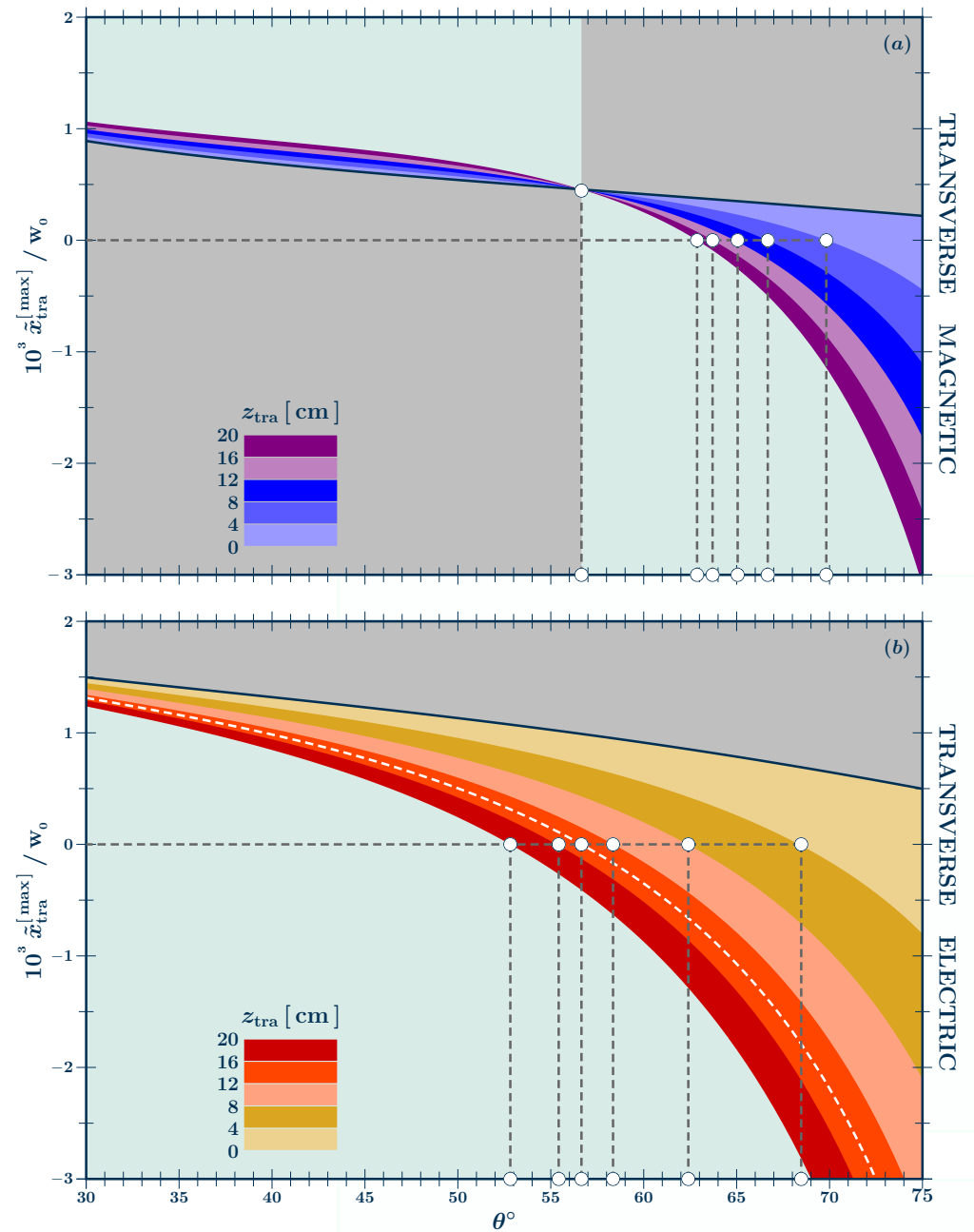
see Figure 4b. For transverse magnetic waves, the compensation happens for incidence angles greater than the Brewster angle, $\theta_{\text{B}} = 56.65°$. For incidence angles of

$$60°, 65°, 70° \; ,$$

angular deviations compensate for the GH shifts at the axial distances

$$50.68, 11.68, 3.88 \;\; \text{cm} \; ,$$

see Figure 4a.

Figure 3. GH shift and angular deviations as functions of the incidence angle for different axial distances. The displacement of the maximum of the upper transmitted beam is plotted for transverse magnetic and electric waves, respectively in (**a**,**b**). In (**a**), at Brewster incidence, $\theta_B = 56.65°$, the axial dependence is removed. In (**b**), for Brewster incidence, angular deviations compensate for the GH shift at an axial distance of 14.14 cm (the white dashed line). The colored zones refer to different axial distances. In (**a**,**b**), we also find the incidence angle for which these optical effects offset each other.
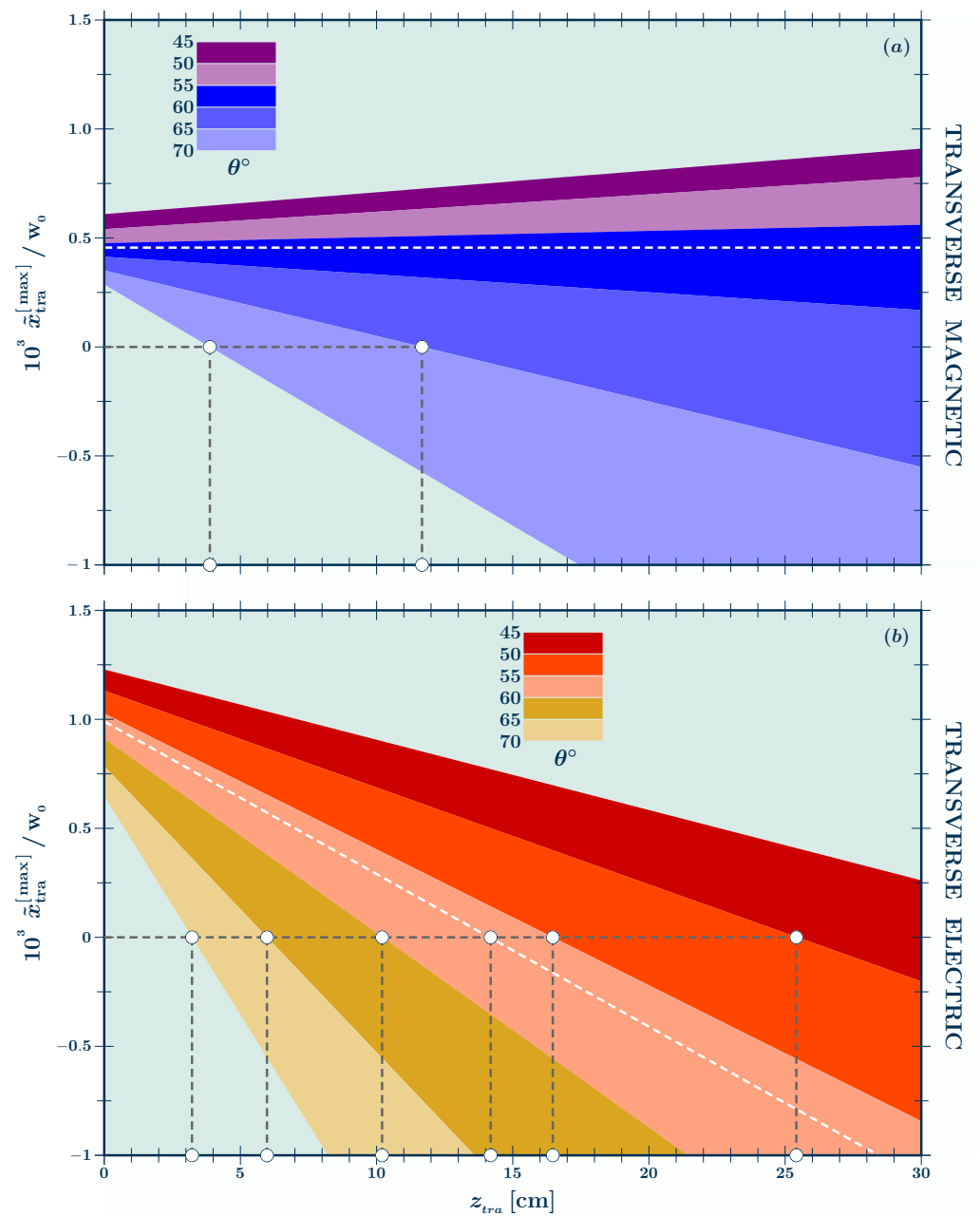
Figure 4. GH shift and angular deviations as functions of the axial distance for different incidence angles. In (**a**,**b**), the white dashed line refers to the Brewster incidence. For transverse magnetic waves, no axial dependence is seen. For electric waves, angular deviations compensate the GH shift at an axial distance of 14.14 cm. The colored zones refer to different incidence angles. In (**a**,**b**), we also find the axial distance for which these optical effects offset each other.

6. Discussions

Lateral displacements of optical beams with respect to the path predicted by geometric optics stimulated, in the last decades, both theoretical and experimental investigations. Two types of displacements characterize the transmission through dielectric blocks. The first, known as the GH shift, is due to the phase of the total internal reflection coefficient and it is independent of the axial position of the detector. The second one is due to the modulation of the transmission coefficients on the wave number distribution of the incident beam and it is dependent on the axial position of the detector.

In region III, far enough from the critical region II, GH shifts are proportional to the wavelength of the optical beam. When the axial distance also approaches the Rayleigh axial

range, the angular deviations become proportional to the wavelength and this opens the doors to the possibility to cancel the lateral displacements induced by the total reflection coefficient. This phenomenon is also known as the composite GH effect [25,26]. In region I, where the partial internal reflection implies the only presence of angular deviations [27] an amplification effect happens near the internal Brewster angle, for details see Ref. [23]. Region II represents the region around the critical angle and an amplification by a factor $\sqrt{|\boldsymbol{k}|\,\mathrm{w}_0}$, see Equation (11), is found in proximity of the critical incidence [8,24]. Such a region is also characterized by oscillatory phenomena [20–22] and the analytical formula, obtained in this paper for the intensity of the upper transmitted beam, i.e Equation (8), fails to reproduce the numerical data. It is important to observe here that region II represents a very small region of the incidence spectrum covering a range of $8/|\boldsymbol{k}|\,\mathrm{w}_0$ around the critical angle. This means, for a beam waist of 100 μm and a wavelength of 532 nm, a range of 0.4° around the critical angle. Consequently, the analytical formula presented in this paper is in excellent agreement with the numerical data for all the incidence angles greater than $\theta_c + 4/|\boldsymbol{k}|\,\mathrm{w}_0$, or in the case of the beam parameters used in our simulations, for incidence angles greater than $\theta_c + 0.4°$.

7. Conclusions And Outlooks

In this paper, by using the Taylor expansion of the Fresnel coefficients of the transmission through the first and third interfaces and of the total reflection by the second interface, we have given an analytical expression for the upper transmitted beam intensity, see Equation (8). From this analytical approximation, it is immediate to obtain the cubic equation to calculate the intensity maximum. The cubic equation (9) can then be further reduced to a linear equation (10), from which we can obtain the incidence angles and axial distances for which GH shifts and angular deviations offset each other. For transverse magnetic waves, this compensation effect is only possible for incidence greater than the Brewster incidence, $\theta_{\mathrm{B}} = \arctan[n]$.

The analytical expression of the upper transmitted beam given in this paper, see Equation (6), is also useful in view of experimental implementations done by using the weak measurements technique [25,28]. This technique is based on the interference between transverse electric and magnetic waves [29–31]. Consequently, the analytical expression for the upper transmitted beam is important to find the main maximum of the combined optical beam, which is a function of the different lateral displacements and angular deviations of transverse electric and magnetic waves. For the incidence angles and axial distances for which these optical effects offset each other, the weak measurement breaks down because the double peak phenomenon is no longer present. In a forthcoming paper, we shall revise the weak measurements for transmission through dielectric blocks in view of the analytical expression given in this article.

Author Contributions: Conceptualization, methodology, and writing by S.D.L. All the authors contributed in equal form to software, mathematical and graphical analysis, and investigation. All authors have read and agreed to the published version of the manuscript.

Institutional Review Board Statement: Not applicable.

Informed Consent Statement: The study did not involve humans.

Data Availability Statement: The data that support the findings of this study are available from the corresponding author, S.D.L., upon reasonable request.

collaboration between the State University of Campinas (Brazil) and the Salento University of Lecce (Italy).

Conflicts of Interest: The authors declare no conflict of interest.

References

1. Born, M.; Wolf, E. *Principles of Optics*; Cambridge UP: Cambridge, UK, 1999.
2. Sharma, K.K. *Optics: Principles and Applications*; Academic Press: Cambridge, MA, USA, 2006.
3. Saleh, B.E.A.; Teich, M.C. *Fundamentals of Photonics*; Wiley & Sons: Hoboken, NJ, USA, 2007.
4. Goos, F.; Hänchen, H. Ein neuer und fundamentaler Versuch zur Totalreflexion. *Ann. Phys.* **1947**, *436*, 333–346. [CrossRef]
5. Artmann, K. Berechnung der Seitenversetzung des totalreflektierten Strahles. *Ann. Phys.* **1948**, *437*, 87–102. [CrossRef]
6. Horowitz, B.R.; Tamir, T. Lateral Displacement of a Light Beam at a Dielectric Interface. *JOSA* **1971**, *61*, 586–594. [CrossRef]
7. Lai, H.M.; Cheng, F.C.; Tang, W.K. Goos–Hänchen effect around and off the critical angle. *JOSA A* **1986**, *3*, 550–557. [CrossRef]
8. Araújo, M.P.; De Leo, S.; Maia, G.G. Closed-form expression for the Goos-Hänchen lateral displacement. *Phys. Rev. A* **2016**, *93*, 023801. [CrossRef]
9. Ra, J.W.; Bertoni, H.L.; Felsen, L.B. Reflection and transmission of beams at a dielectric interface. *SIAM J. Appl. Math.* **1973**, *24*, 396–413. [CrossRef]
10. Merano, M.; Aiello, A.; 't Hooft, G.W.; van Exter, M.P.; Eliel, E.R.; Woerdman, J.P. Observation of Goos-Hänchen Shifts in Metallic Reflection. *Opt. Express* **2007**, *15*, 15928–15934. [CrossRef]
11. Kogelnik, H.; Weber, H.P. Rays, Stored Energy, and Power Flow in Dielectric Waveguides. *JOSA* **1974**, *64*, 174–185. [CrossRef]
12. Prajapati, C.; Ranganathan, D. Goos-Hänchen and Imbert- Federov Shifts for Hermite-Gauss Beams. *JOSA A* **2012**, *29*, 1377–1382. [CrossRef]
13. Liu, F.P.; Meng, X.J.; Xiao, J.Q.; Wang, A.L.; Yang, C.C. The Goos-Hänchen Shift of Wide-angle Seismic Reflection Wave. *Sci. China Earth Sci.* **2012**, *55*, 852–857. [CrossRef]
14. De Leo, S.; Kraus, R. Incidence Angles Maximizing the Goos-Haenchen Shift in Seismic Data Analysis. *Pure Appl. Geoph.* **2018**, *175*, 2023–2044. [CrossRef]
15. Madrazo, A.; Nieto-Vesperinas, M. Detection of subwavelength Goos–Hänchen shifts from near-field intensities: A numerical simulation. *Opt. Lett.* **1995**, *20*, 2445–2447. [CrossRef] [PubMed]
16. Wang, X.; Yin, C.; Sun, J.; Li, H.; Wang, Y.; Ran, M.; Cao, Z. High-sensitivity temperature sensor using the ultrahigh order mode-enhanced Goos-Hänchen effect. *Opt. Express* **2013**, *21*, 13380–13385. [CrossRef] [PubMed]
17. Nie, Y.; Li, Y.; Wu, Z.; Wang, X.; Yuan, W.; Sang, M. Detection of chemical vapor with high sensitivity by using the symmetrical metal-cladding waveguide-enhanced Goos-Hänchen shift. *Opt. Express* **2014**, *22*, 8943–8948. [CrossRef]
18. Carvalho, S.A.; De Leo, S. The use of the stationary phase method as a mathematical tool to determine the path of optical beams. *Am. J. Phys.* **2015**, *83*, 249–255. [CrossRef]
19. Kompanets, V.; Melnikov, A.; Chekalin, S. Goos-Hänchen shift of a mid-infrared femtosecond filament visualized by the laser coloration method. *Laser Phys. Lett.* **2021**, *18*, 015302–5. [CrossRef]
20. Araújo, M.P.; De Leo, S.; Maia, G.G.Oscillatory behavior of light in the composite Goos-Hänchen shift. *Phys. Rev. A* **2017**, *95*, 053836-9. [CrossRef]
21. Santana, O.; de Araujo, S.E.E. Direct measurement of the composite Goos–Hänchen shift of an optical beam. *Opt. Lett.* **2018**, *43*, 4037–4040. [CrossRef] [PubMed]
22. Santana, O.; de Araujo, S.E.E. Oscillatory trajectory of an optical beam propagating in free space. *Opt. Lett.* **2019**, *44*, 646–649. [CrossRef]
23. Leo, S.D.; Stefano, A. Angular deviations: From a cubic equation to a universal closed formula to determine the peak position of reflected and (upper) transmitted beams. *Eur. Phys. J. Plus* **2021**, *136,* 507–520. [CrossRef]
24. Araújo, M.P.; Carvalho, S.A.; De Leo, S. The frequency crossover for the Goos-Hänchen shift. *J. Mod. Opt.* **2013**, *60*, 1772–1780. [CrossRef]
25. Santana, O.J.; Carvalho, S.A.; De Leo, S.; de Araújo, L.E.E. Weak measurement of the composite Goos-Hänchen shift in the critical region. *Opt. Lett.* **2016**, *41*, 3884–3887. [CrossRef]
26. Olaya, C.M.; Hayazawa, N.; Hermosa, N.; Tanaka, T. Angular Goos-Hänchen shift sensor using a gold film enhanced by surface plasmon resonance. *J. Phys. Chem. A* **2021**, *125*, 451–458. [CrossRef]
27. Xu, Y.; Wu, L.; Ang, L.K. Ultrasensitive optical temperature transducers based on surface plasmon resonance enhanced composited Goos-Hänchen and Imbert-Fedorov shifts. *IEEE J. Sel. Top. Quantum Electron.* **2021**, *27*, 4601508-8. [CrossRef]
28. Goswami, S.; Pal, M.; Nandi, A.; Panigrahi, P.K.; Ghosh, N. Simultaneous weak value amplification of angular Goos–Hänchen and Imbert–Fedorov shifts in partial reflection. *Opt. Lett.* **2014**, *39*, 6229–6232. [CrossRef] [PubMed]
29. Araújo, M.; De Leo, S.; Maia, G. Optical weak measurements without removing the Goos-Haenchen phase. *J. Mod. Opt.* **2018**, *65*, 837–846. [CrossRef]
30. Araújo, M.P.; De Leo, S.; Maia, G.G. Optimizing weak measurements to detect angular deviations. *Ann. Phys.* **2017**, *529*, 1600357-20. [CrossRef]
31. De Leo, S.; Maia, G. Lateral shifts and angular deviations of Gaussian optical beams reflected by and transmitted through dielectric blocks: A tutorial review. *J. Mod. Opt.* **2019**, *66*, 2142–2194. [CrossRef]